DTU Library

Fluxons in thin-film superconductor-insulator superlattices

Sakai, S.; Bodin, P.; Pedersen, Niels Falsig

Link back to DTU Orbit

Fluxons in thin-film superconductor-insulator superlattices

S. Sakai and P. Bodin
Electrotechnical Laboratory, 1-1-4 Umezono, Tsukuba-shi, Ibaraki 305, Japan

N. F. Pedersen
Physics Laboratory I, Technical University of Denmark, DK-2800 Lyngby, Denmark

In a system of thin alternating layers of superconductors and insulators the equations describing static and dynamic fluxon solutions are derived. The approach, represented by a useful compact matrix form, is intended to describe systems fabricated for example of niobium or niobium-nitride thin films; in the limit of ultrathin superconductor films it may give a model for describing fluxon motion in layered high-T_c superconductors. Numerical examples of current versus voltage curves to be expected in such an experiment are presented.

I. INTRODUCTION

Systems of many closely coupled Josephson junctions are being considered for many applications of superconducting electronics. Examples are found in the Josephson voltage standard, in the Josephson computer, and in microwave generators based on coherent action of many junctions. Large networks of Josephson junctions have also received much attention as model systems for phase transitions and for fluxon propagation.

All such work is characterized by the problem of creating many interacting or closely coupled junctions in the two-dimensional plane defined by the substrate. Here we want to address the problem of "vertical" integration of Josephson junction systems. Basic to this idea is, of course, the fact that closely interacting systems are much easier to obtain in three dimensions than in two or one dimensions. So far the applications of three-dimensional circuits of Josephson junctions in niobium-type superconducting electronics are rare, although experimental circuits with three layers of superconductors and two oxide barrier layers are known with small area junctions;[1] with long Josephson junctions some experiments have taken place[2] or are in progress.[3]

A promising avenue toward many electronic applications of thin-film superconductivity is the use of fluxons[4,5] in long Josephson junctions. Examples here are the phase mode superconducting computer[6] and cavity coupled phase-locked long Josephson junctions as microwave generators.[7-9] For such circuits the problem of designing large systems of closely interacting long Josephson junctions in two dimensions is very difficult—even more so than for small junctions. Hence, it is of interest to study the properties of fluxon propagation in stacked layers of superconductors. In this article we will consider the case where the thickness of the superconducting layers is smaller than or comparable to the London penetration depth so that there is a large coupling perpendicular to the layers. As we shall see, a fluxon can then extend over many layers. Recent experimental data[10] suggest that oxide superconductors with strong anisotropy between the c axis and a or b axis, e.g., Bi-Sr-Ca-Cu-O compounds, consist of Josephson-coupled Cu-O superconducting layers.[11] Recent theories[12,13] based on the Lawrence and Doniach model,[14] where stacked zero-thickness superconducting planes are coupled by the Josephson tunneling effect, mainly discuss static flux lattice structure of such highly anisotropic oxide superconductors. Our model includes time dependence and has no limitations to the superconductor film thicknesses, so it may be a good model for describing fluxon dynamics in such oxide superconductor systems. We specialize our results to geometries that are well known from traditional experiments using low-T_c metal superconductors, such as the in-line and overlap geometries. We also present numerical calculations of current versus voltage (I-V) curves relating to systems that could be fabricated in niobium or niobium-nitride technology.

The article is organized in the following way. In Sec. II we present a theory describing electromagnetic wave motion for our layered superconductor and present some specialized examples such as the in-line and overlap junctions. Section III discusses coherent fluxon solutions and gives some numerical calculations of fluxon statics and dynamics with I-V curves for comparison to future experiments. Finally, conclusions are given in Sec. IV.

II. THE LAYERED SUPERCONDUCTOR MODEL

Figure 1(a) shows our superconductor-insulator model system, an $SISISI \cdots IS$ structure. The ith superconducting layer (S layer) has a thickness t_i and a London penetration depth λ_i, and the thickness of the insulating layer between S layers i and $i-1$ is $d_{i,i-1}$. The structure has a length l in the x direction and a width W in the y direction. In the following all the physical quantities such as currents, magnetic field, etc. will be characterized by index i, relating to the ith superconductor layer.

Figure 1(b) shows in more detail the S layers i and $i-1$, for which we may derive the current density J_i^L in the bottom of the ith S layer,

$$J_i^L = -\frac{1}{2e\mu_0\lambda_i^2}(\hbar\nabla\theta_i + 2eA_i), \tag{1}$$

where A_i is the vector potential and θ_i is the phase of the macroscopic wave function for the ith S layer. Here we asuume that the properties of the S layers are described only by the phase. This corresoponds to a circumstance of low-magnetic-field application. Therefore, the normal core
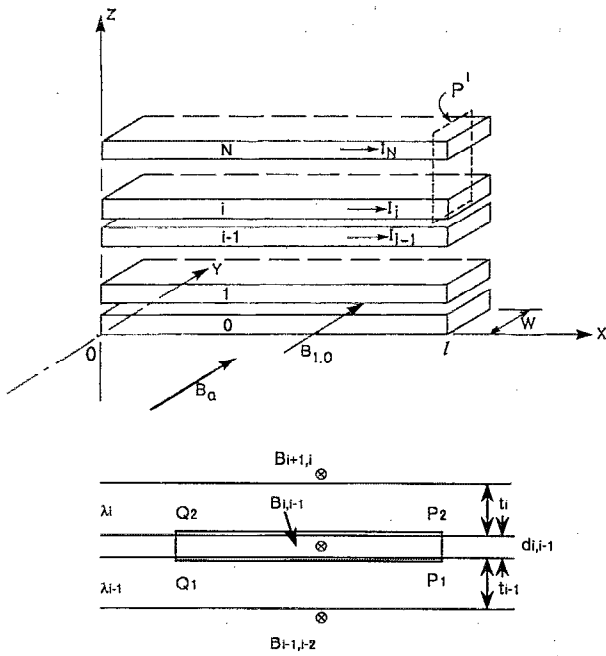
FIG. 1. (a) Schematic diagram of the long Josephson junction superlattice. (b) Detail of S layers i and $i-1$.

of the flux quantum can exist in the insulating layers as a Josephson vortex, but the case where it penetrates into the S layers is excluded. The gauge invariant phase difference between S layers i and $i-1$ may then be written

$$\phi_{i,i-1}(x) = \theta_i - \theta_{i-1} + \frac{2e}{\hbar} \int_{Q_1}^{Q_2} \mathbf{A} \cdot \mathbf{dl}, \quad (2)$$

where we assume that the phase θ_i does not change in the z direction in the S layer. The current density to the z direction is of the order of the Josephson current density, but the density to the x direction can be a level of the critical density of the S layer itself. Usual cases are that the latter is much higher than the former. Thus the phase change to the z direction in the S layer can be ignored.

The magnetic flux through the area $P_1P_2Q_2Q_1$ in Fig. 1(b) is then

$$\Phi = \int B_{i,i-1} \, dS = \oint \mathbf{A} \cdot \mathbf{dl}. \quad (3)$$

After some lengthy but straightforward calculations we obtain the equation

$$\frac{\partial \phi_{i,i-1}}{\partial x} = -\frac{2e}{\hbar} d_{i,i-1} B_{i,i-1} - \frac{2e\mu_0\lambda_i^2}{\hbar} J_i^L + \frac{2e\mu_0\lambda_{i-1}^2}{\hbar} J_{i-1}^U, \quad (4)$$

where $B_{i,i-1}$ is the magnetic-flux density between S layers i and $i-1$. Following our notation J_{i-1}^U is the current density in the upper part of S layer $i-1$. Inside S layer i, the magnetic-flux density (in the y direction) is described, in our model, by

$$\frac{\partial^2 B}{\partial z^2} = \frac{1}{\lambda_i^2} B. \quad (5)$$

By using Eq. (5) and the magnetic-flux density in the neighboring I layer (insulating layer) the surface currents J_i^L and J_{i-1}^U may now be expressed:

$$J_i^L = \frac{1}{\mu_0\lambda_i} \frac{B_{i,i-1} \cosh(t_i/\lambda_i) - B_{i+1,i}}{\sinh(t_i/\lambda_i)}, \quad (6a)$$

$$J_{i-1}^U = \frac{1}{\mu_0\lambda_{i-1}} \frac{B_{i-1,i-2} - B_{i,i-1} \cosh(t_{i-1}/\lambda_{i-1})}{\sinh(t_{i-1}/\lambda_{i-1})}. \quad (6b)$$

From Eqs. (4) and (6) we can now obtain the simple relation

$$-\frac{\hbar}{2e} \frac{\partial \phi_{i,i-1}}{\partial x} = d'_{i,i-1} B_{i,i-1} + s_i B_{i+1,i} + s_{i-1} B_{i-1,i-2}, \quad (7)$$

where we have defined the effective magnetic thickness $d'_{i,i-1}$,

$$d'_{i,i-1} = d_{i,i-1} + \lambda_i \coth\left(\frac{t_i}{\lambda_i}\right) + \lambda_{i-1} \coth\left(\frac{t_{i-1}}{\lambda_{i-1}}\right), \quad (8a)$$

and the parameter s_i describing the coupling between layers by

$$s_i = -\frac{\lambda_i}{\sinh(t_i/\lambda_i)}. \quad (8b)$$

With the definitions in Eq. (8), Eq. (7) may be written in the compact matrix form

$$-\frac{\hbar}{2e}\frac{\partial}{\partial x}
\begin{bmatrix} \phi_{1,0} \\ \phi_{2,1} \\ \vdots \\ \phi_{i,i-1} \\ \vdots \\ \phi_{N,N-1} \end{bmatrix}
=
\begin{bmatrix}
s_0 & d'_{1,0} & s_1 & 0 & \cdots & & & \\
0 & s_1 & d'_{2,1} & s_2 & 0 & \cdots & & \\
 & & \ddots & \ddots & \ddots & & & \\
 & & 0 & s_{i-1} & d'_{i,i-1} & s_i & 0 & \\
 & & & & \ddots & \ddots & \ddots & \\
 & & & & & \ddots & \ddots & \ddots & 0 \\
 & & & & & 0 & s_{N-1} & d'_{N,N-1} & s_N
\end{bmatrix}
\begin{bmatrix} B_{0,-1} \\ B_{1,0} \\ \vdots \\ B_{i,i-1} \\ \vdots \\ B_{N,N-1} \\ B_{N+1,N} \end{bmatrix}. \quad (9)$$

At the bottom and top of our structure [Fig. 1(a)] we have introduced the extra magnetic fields $B_{0,-1}$ and $B_{N+1,N}$, respectively. This implies that the tensor in Eq. (9) gets the dimensions $N \times (N+2)$. In the case of an applied uniform magnetic-flux density B_a we have $B_{0,-1} = B_{N+1,N} = B_a$.
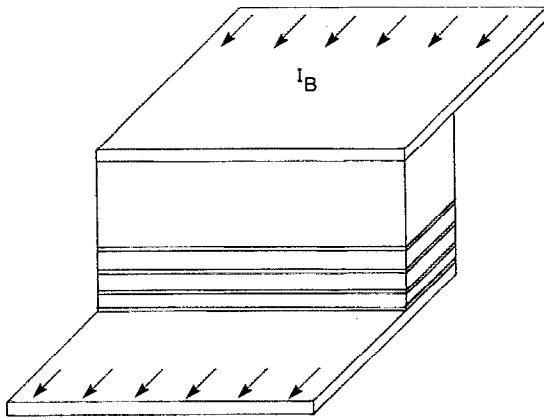
If we consider the closed path P' in Fig. 1(a) we note that all the currents inside P' contribute to the magnetic flux density $B_{i,i-1}$. This is understood from $\nabla \times \mathbf{H} = \mathbf{J}$, giving rise to

$$B_{i,i-1} = \frac{\mu_0}{W} \sum_{k=i}^{N} I_k + B_a . \tag{10}$$

Using Eq. (10) we may rewrite Eq. (9) to the useful form

$$-\frac{\hbar}{2e} \frac{\partial}{\partial x} \begin{pmatrix} \phi_{1,0} \\ \phi_{2,1} \\ \vdots \\ \phi_{i,i-1} \\ \vdots \\ \vdots \\ \phi_{N,N-1} \end{pmatrix} = \frac{\mu_0}{W} \begin{pmatrix} d'_{1,0} & d'_{1,0}+s_1 & d'_{1,0}+s_1 & \cdots & \cdots & d'_{1,0}+s_1 & d'_{1,0}+s_1 \\ s_1 & d'_{2,1}+s_1 & d'_{2,1}+s_1+s_2 & \cdots & \cdots & d'_{2,1}+s_1+s_2 & d'_{2,1}+s_1+s_2 \\ 0 & s_2 & d'_{3,2}+s_2 & & & & \\ \vdots & 0 & & \ddots & \ddots & & \\ & & & & \ddots & & \\ & & & \cdots & 0 & s_{N-1} & d'_{N,N-1}+s_{N-1} \end{pmatrix} \begin{pmatrix} I_1 \\ I_2 \\ \vdots \\ \vdots \\ I_N \end{pmatrix}$$

$$+ B_a \begin{pmatrix} d'_{1,0}+s_1+s_0 \\ d'_{2,1}+s_1+s_2 \\ \vdots \\ d'_{N,N-1}+s_{N-1}+s_N \end{pmatrix} . \tag{11}$$

From the usual Josephson junction model we now introduce the capacitive, resistive, and Josephson current between S layers i and $i-1$, and we define the total current of them, $J^Z_{i,i-1}$ by

$$J^Z_{i,i-1} \equiv \frac{\hbar}{2e} C_{i,i-1} \frac{\partial^2 \phi_{i,i-1}}{\partial t^2} + \frac{\hbar}{2e} G_{i,i-1} \frac{\partial \phi_{i,i-1}}{\partial t} + J_{i,i-1} \sin \phi_{i,i-1} . \tag{12a}$$

Here $C_{i,i-1}$ is the unit area capacitance, $G_{i,i-1}$ the unit area conductivity, and $J_{i,i-1}$ the dc maximum Josephson current density between S layers i and $i-1$.

We can now write

$$-\frac{1}{W} \frac{\partial I_i}{\partial x} = J^Z_{i,i-1} - J^Z_{i+1,i} \quad \text{for} \quad 1 \leqslant i \leqslant N-1,$$

and

$$-\frac{1}{W} \frac{\partial I_N}{\partial x} = J^Z_{N,N-1} . \tag{12b}$$

We note here that an external bias current may be added to the right-hand side of Eq. (12b) if necessary. Combining Eqs. (11) and (12) we obtain the very general equation

$$\frac{\hbar}{2e\mu_0} \frac{\partial^2}{\partial x^2} \begin{pmatrix} \phi_{1,0} \\ \vdots \\ \phi_{i,i-1} \\ \vdots \\ \phi_{N,N-1} \end{pmatrix} = \begin{pmatrix} d'_{1,0} & s_1 & 0 & \cdots & & & \\ s_1 & d'_{2,1} & s_2 & 0 & \cdots & & \\ & & \ddots & & & & \\ & 0 & s_{i-1} & d'_{i,i-1} & s_i & 0 & \\ & & & & \ddots & & \\ & & & & & s_{N-1} & \\ & & & 0 & s_{N-1} & d'_{N,N-1} \end{pmatrix} \begin{pmatrix} J^Z_{1,0} \\ \vdots \\ J^Z_{i,i-1} \\ \vdots \\ J^Z_{N,N-1} \end{pmatrix} , \tag{13}$$

where $J^Z_{i,i-1}$ is defined in Eq. (12a). If the applied magnetic field B_a is uniform it does not appear in the equations, but appears in the boundary conditions at $x=0$ and $x=l$. They become

FIG. 2. The N-layer overlap junction.

$$-\frac{\hbar}{2e}\frac{\partial}{\partial x}\begin{pmatrix}\phi_{1,0}\\ \vdots\\ \phi_{i,i-1}\\ \vdots\\ \phi_{N,N-1}\end{pmatrix}_{\substack{x=0\\x=L}} = B_a\begin{pmatrix}s_0+d'_{1,0}+s_1\\ \vdots\\ s_{i-1}+d'_{i,i-1}+s_i\\ \vdots\\ s_{N-1}+d'_{N,N-1}+s_N\end{pmatrix}. \qquad (14)$$

For the usual long Josephson junctions with only two superconducting layers we are used to distinguishing between overlap junctions and in-line junctions. In the present system the closest equivalent to an overlap junction would be a case in which a bias current I_B is supplied uniformly to the Nth layer and taken out uniformly in the zeroth layer as shown schematically in Fig. 2. In that case the vector

$$-I_B\begin{pmatrix}d'_{1,0}+s_1\\ d'_{2,1}+s_1+s_2\\ \vdots\\ d'_{N-1,N-2}+s_{N-2}+s_{N-1}\\ d'_{N,N-1}+s_{N-1}\end{pmatrix} \qquad (15)$$

should be added to the right-hand side of Eq. (13).

For the in-line case shown in Fig. 3 the magnetic-flux density at the upper side of the top bias lead is $-(\mu_0/2W)I_C$, where I_C is the bias current and at the lower side of the structure it is $+(\mu_0/2W)I_C$. Equation (10) then becomes
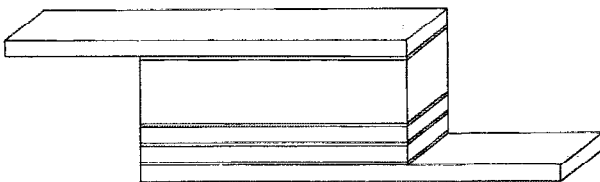
FIG. 3. The N-layer in-line junction.

$$B_{i,i-1}=\frac{\mu_0}{W}\sum_{k=i}^{N}I_k-\frac{\mu_0}{2W}I_C, \qquad (16)$$

with the condition $\Sigma_{k=0}^N I_k=I_C$. The second term on the right-hand side of Eq. (11) is now changed to

$$-\frac{\mu_0}{2W}I_C\begin{pmatrix}d'_{1,0}+s_1-s_0\\ d'_{2,1}+s_1+s_2\\ \vdots\\ d'_{N,N-1}+s_{N-1}+s_N\end{pmatrix}. \qquad (17)$$

This term is independent of x so that the wave equation is basically the same as Eq. (13). The effect of I_C appears only in the different boundary conditions at $x=0$ and $x=l$. These are at $x=0$, $I_N=I_C$, and $I_i=0$, for $0\leqslant i\leqslant N-1$, i.e.,

$$\frac{\partial}{\partial x}\begin{pmatrix}\phi_{1,0}\\ \vdots\\ \vdots\\ \phi_{N-1,N-2}\\ \phi_{N,N-1}\end{pmatrix}_{x=0}=-\frac{\mu_0 e I_C}{\hbar W}\begin{pmatrix}s_0+d'_{1,0}+s_1\\ \vdots\\ \vdots\\ s_{N-2}+d'_{N-1,N-2}+s_{N-1}\\ s_{N-1}+d'_{N,N-1}-s_N\end{pmatrix},$$
(18a)

and at $x=l$, $I_0=I_C$, and $I_i=0$, for $1\leqslant i\leqslant N$, i.e.,

$$\frac{\partial}{\partial x}\begin{pmatrix}\phi_{1,0}\\ \phi_{2,1}\\ \vdots\\ \vdots\\ \phi_{N,N-1}\end{pmatrix}_{x=l}=\frac{\mu_0 e I_C}{\hbar W}\begin{pmatrix}-s_0+d'_{1,0}+s_1\\ s_1+d'_{2,1}+s_2\\ \vdots\\ \vdots\\ s_{N-1}+d'_{N,N-1}+s_N\end{pmatrix}. \qquad (18b)$$

III. SELECTED EXAMPLES

In the following we will illustrate some of the consequences of the general equations derived in the previous section. The numerical part of the examples are selected so that realistic junction parameters are used, and some of the effects predicted should be observable in realistic experiments in niobium or niobium-nitride thin-film systems.

A. The coherence mode

The equations of the previous section have solutions in which fluxons in different layers move synchronously (or phase locked). This is a very interesting type of motion that has been studied in planar systems.[7-9]

For simplicity let us assume three superconducting layers with the bias current of the overlapping geometry as in Fig. 2. We assume that the top and bottom layers have the same properties, and the two insulating layers have equal properties, i.e., $N=3$, $d_{1,0}=d_{2,1}\equiv d$, $t_2=t_0$ (but may be different from t_1), $\lambda_2=\lambda_0$ (but may be different from λ_1). The two tunnel junctions have the same properties described by C, G, and J [Eq. (12a)]. Equations (13) and (15) now become

$$\frac{\hbar}{2e\mu_0}\begin{pmatrix}\dfrac{\partial^2\phi_{1,0}}{\partial x^2}\\[2mm]\dfrac{\partial^2\phi_{2,1}}{\partial x^2}\end{pmatrix}$$

$$=\begin{pmatrix}d' & s\\ s & d'\end{pmatrix}\begin{pmatrix}\dfrac{\hbar C}{2e}\dfrac{\partial^2\phi_{1,0}}{\partial t^2}+\dfrac{\hbar G}{2e}\dfrac{\partial\phi_{1,0}}{\partial t}+J\sin\phi_{1,0}\\[3mm]\dfrac{\hbar C}{2e}\dfrac{\partial^2\phi_{2,1}}{\partial t^2}+\dfrac{\hbar G}{2e}\dfrac{\partial\phi_{2,1}}{\partial t}+J\sin\phi_{2,1}\end{pmatrix}$$

$$-I_B(d'+s)\begin{pmatrix}1\\1\end{pmatrix},\tag{19}$$

where

$$d'=d+\lambda_0\coth(t_0/\lambda_0)+\lambda_1\coth(t_1/\lambda_1)\tag{20a}$$

and

$$s=-\frac{\lambda_1}{\sinh(t_1/\lambda_1)}.\tag{20b}$$

Let us now look for a coherent mode with the property $\phi_{1,0}(x,t)=\phi_{2,1}(x,t)\equiv\phi(x,t)$. In that case Eq. (19) becomes

$$\frac{\hbar}{2e\mu_0}\frac{\partial^2\phi}{\partial x^2}=(d'+s)\left(\frac{\hbar C}{2e}\frac{\partial^2\phi}{\partial t^2}+\frac{\hbar G}{2e}\frac{\partial\phi}{\partial t}+J\sin\phi-I_B\right).\tag{21}$$

This equation is almost the same as the perturbed sine-Gordon equation known from conventional long Josephson junctions.[4] The main difference is a change of the length scale due to the factor $(d'+s)$ in Eq. (21). If we go through the normalizations as, for example, done in Ref. 15, we find that the effective Josephson penetration depth $\lambda_J^{(2)}$ becomes

$$\lambda_J^{(2)}=\left(\frac{\hbar}{2e\mu_0(d'+s)J}\right)^{1/2},\tag{22}$$

and the velocity of light in the barrier $\bar c^{(2)}$

$$\bar c^{(2)}=\frac{1}{\sqrt{\epsilon\mu_0}}\left(\frac{d}{d'+s}\right)^{1/2}.\tag{23}$$

Compared to the single-junction soliton case we note that

$$\frac{\lambda_J^{(2)}}{\lambda_J^{(1)}}=\frac{\bar c^{(2)}}{\bar c^{(1)}}=\left(\frac{d'}{d'+s}\right)^{1/2},\tag{24}$$

where index 1 refers to the single-junction soliton case. Since $s<0$ [Eq. 20(b)] we note that $\bar c^{(2)}$ is larger than $\bar c^{(1)}$, i.e., we may exceed the velocity of light in the single-junction case. A similar conclusion was reached in Ref. 16.

We also note that if we arrange a bias situation such that we extract a bias current I_{B1} from the center layer such that $I_{B1}=-2I_B$ (see Fig. 4) the solutions discussed above become antisymmetric in the sense that, i.e., now a
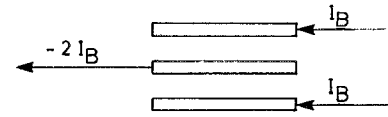

FIG. 4. Schematic diagram of biasing for the coherent soliton-antisoliton mode.

soliton and an antisoliton move together in a coherent mode. The equation of motion and the penetration depth and velocity of light can be obtained from Eqs. (21), (22), and (23) by substituting $-s$ for s. It should be noted that this coherent soliton-antisoliton state is not possible in conventional single long Josephson junctions.

Above we have concentrated on the coherent modes of the $N=3$ system. Of course, other modes than the coherent are possible; an example is shown in Sec. III C.

For $N>3$ we can follow the same procedure as used above. A complication, of course, is the boundaries created by the top and bottom layers. For $N\gg1$ it may be justified to neglect effects from these two layers and assume that all the intervening layers are identical. In that case we may obtain coherent solutions of the same nature as for the $N=3$ case discussed above. For the N layer system ($N\gg1$) each of the $N-1$ coherent solitons will then obey the equation

$$\frac{\hbar}{2e\mu_0}\frac{\partial^2\phi}{\partial x^2}=(d'+2s)\left(\frac{\hbar C}{2e}\frac{\partial^2\phi}{\partial t^2}+\frac{\hbar G}{2e}\frac{\partial\phi}{\partial t}+J\sin\phi-I_B\right),\tag{25}$$

and the characteristic length and velocity are now

$$\lambda_J^{(N-1)}=\left(\frac{\hbar}{2e\mu_0(d'+2s)J}\right)^{1/2},\tag{26a}$$

$$\bar c^{(N-1)}=\frac{1}{\sqrt{\epsilon\mu_0}}\left(\frac{d}{d'+2s}\right)^{1/2}.\tag{26b}$$

B. Single fluxon in the static case

The previous general equations will be illustrated by a numerical example below. For a system consisting of seven junctions ($N=8$) with equal properties we have calculated the phase difference $\phi_{i,i-1}$, the magnetic-flux density $B_{i,i-1}$, and the supercurrent $\sin\phi_{i,i-1}$ for each of the seven junctions. We consider the static case and use the input boundary conditions

$$\left(\frac{\partial\phi_{i,i-1}}{\partial x}\right)_{x=\pm L/2}=0.$$

For the central layer we set $\phi_{4,3}(0)=\pi$, and for the six other junctions $\phi_{i,i-1}(0)=0$. This is equivalent to assuming that only in the middle layer do we have a fluxon. Such
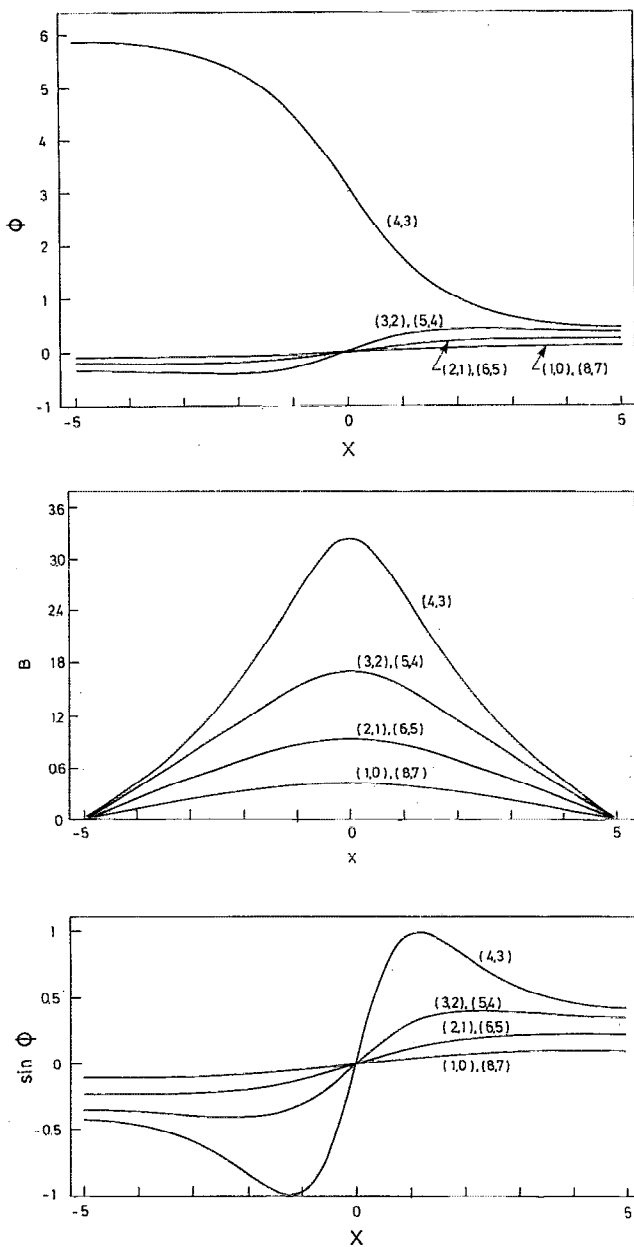
FIG. 6. Calculated I-V curves for the (a) symmetric and (b) coherent modes in an $N=3$ system. $L=5$, $\alpha=0.1$, $S=-0.3$. Voltage for one junction is shown.

fluxon to be distributed over all layers. Figure 5(c) shows the Josephson current distribution in the different layers. From Fig. 5(c) we note that the width of the fluxon has increased compared to the single-junction case,[17] in qualitative agreement with Eqs. (22) and (26).

Note that the static case expression of Eq. (13), obtained by neglecting the time-dependent terms in Eq. (12a), has an analogous form to that of the Bulaevskii and Clem theory[12] based on the Lawrence and Doniach model. $2e\mu_0 Jd'/\hbar$ and $2e\mu_0 Js/\hbar$ of our notation correspond to $2/\lambda_J^2 + 1/\lambda_c^2$ and $-1/\lambda_J^2$ of their notation, respectively [see Eq. (4) in Ref. 12].

C. Coherence of the two-fluxon case

We have made numerical simulations corresponding to the two-fluxon coherent state described in Eq. (21). The normalizations are performed using the usual one-soliton case with the velocity of light given by $\bar{c}^{(1)}$ and the Josephson penetration depth $\lambda_J^{(1)}$. The parameters are: $N=3$ (two junctions), $\alpha=0.1$, $L=5$, and the coupling parameter $S=-0.3$, where the loss α is defined by $\alpha=G(\hbar/2eCJ)^{1/2}$ under the normalization. The initial condition is two identical fluxons—one in each of the junctions. Figure 6 shows the static I-V curve for the coherent two-junction mode. Also shown is another mode we found during the simulations, particularly for low bias current, the symmetric mode. For this mode the motion is symmetric in the sense that when the fluxon in junction (0.1) is at $x=L$ then the fluxon in junction (2.1) is at $x=0$ The wave form is shown in Fig. 7(a), and we note that the two solitons perturb each other even though they are in different junctions. We also note from Fig. 6 that the asymptotic voltage is apparently somewhat smaller than that of the one-junction case, which is given by $V_s=2\pi/L$.

For the coherent mode in Fig. 6 the asymptotic value of the voltage is approximately 1.20 times higher that of the single-junction case. This factor is in very good agreement with $\bar{c}^{(2)}/\bar{c}^{(1)} = 1/\sqrt{1+S}$ [Eq. (24)].

We note that the losses appear to play a bigger role for the symmetric mode. Even though the solitons are in dif-

FIG. 5. Static one-fluxon solution. $N=8$, $L=10$. The numbering $(i,i-1)$ for each curve refers to the different layers. The coupling parameter $S\equiv s/d'=-0.4997$ (strong coupling). (a) The phase difference $\phi_{i,i-1}$, (b) the magnetic field $B_{i,i-1}$, and (c) the supercurrent $\sin\phi_{i,i-1}$.

a static-type solution may be physically stable in a model with fluctuations of junction parameters, as was demonstrated in a single-junction case.[17]

Figure 5(a) shows the phase difference for the different layers (note that layers 1.0 and 8.7, 2.1 and 6.5, and 3.2 and 5.4 are identical for reasons of symmetry). The parameters are: $L\equiv l/\lambda_J^{(1)}=10$, $S\equiv s/d'=-0.4997$ corresponding to strong coupling. As is evident from Fig. 5(a) we obtain phase changes for the noncentral layers due to the current flowing in the different layers. Figure 5(b) shows the corresponding magnetic-flux density in the insulating layers. Also here the values of the magnetic field in the noncentral layers are significant, and we may consider the
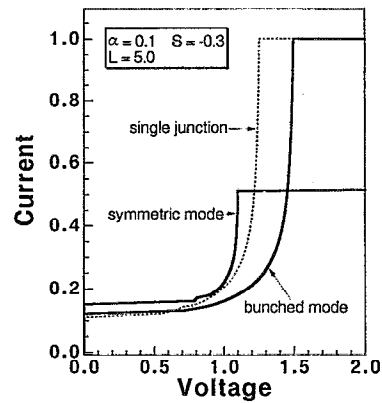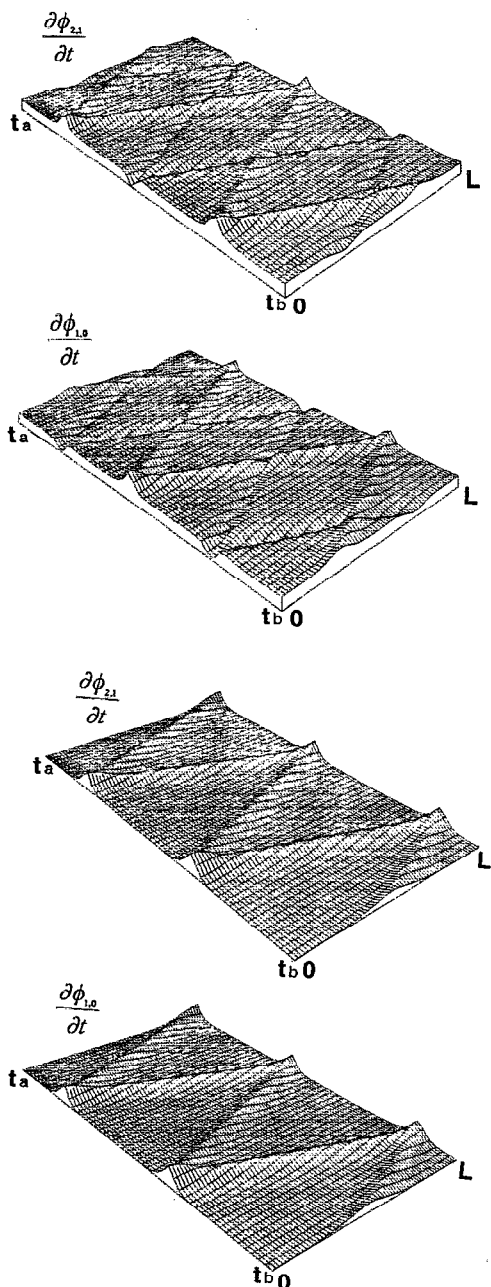
$$\frac{\partial \phi_{2,1}}{\partial t}$$

$$\frac{\partial \phi_{1,0}}{\partial t}$$

$$\frac{\partial \phi_{2,1}}{\partial t}$$

$$\frac{\partial \phi_{1,0}}{\partial t}$$

FIG. 7. Wave forms for (a) symmetric mode at $i_B \equiv I_B/J = 0.4$ and (b) coherent mode at $i_B = 0.4$, corresponding to Fig. 6. $L = 5$, $\alpha = 0.1$, $S = -0.3$. Time is normalized to $\lambda_J^{(1)}/\bar{c}^{(1)}$, and $t_b - t_a = 20$.

ferent lines, they interact with each other, and "pseudocollisions" take place as can be seen from Fig. 7(a).

The line shape for the coherent mode is shown in Fig. 7(b). Here it should be noted that the two solitons are fully identical, i.e., there is no phase shift between them, as is usually the case for coherent modes in other comparable systems.[18]

The behavior resembles qualitatively the system of two solitons in one junction with surface losses.[18] Also, here both the bunched and the symmetric modes exist, although their stability ranges are distinctly different from those in Fig. 6; however, in both cases high bias seems to favor the coherent or bunched mode.

Transitions between the two modes may take place of course, and which one we get depends on the initial conditions. This will be the subject of further studies.[19]

IV. CONCLUSION

A system consisting of alternating layers of superconducting and insulating thin films has been considered. We assume the dimensions in the plane to be large so that the system resembles stacked long Josephson junctions. An implicit assumption is that the film thickness is not large compared to the London penetration depth. This condition can be readily met in niobium-nitride or niobium systems.

Our analysis shows a variety of interesting behavior; of particular interest is the mode of $N - 1$ coherent solitons in a structure with N superconducting layers. This mode may have practical interest in connection with phase locking of Josephson oscillators. Other types of motion that we observed in numerical simulations are unique to the three-dimensional structure, and do not exist in the one- or two-dimensional sine-Gordon systems that have mostly been considered until now.

[1] M. G. Blamire, E. C. G. Kirk, R. E. Somekh, and J. E. Evetts, J. Appl. Phys. **69**, 2376 (1991).

[2] K. Yoshida, K. Kudo, M. S. Hossain, and K. Enpuku, IEEE Trans. Magn. **MAG-27**, 2696 (1991).

[3] G. Costabile and P. Barbara (private communication).

[4] N. F. Pedersen, IEEE Trans. Magn. **MAG-27**, 3328 (1991).

[5] S. Sakai, in *High Temperature Superconductivity and Localisation Phenomena*, edited by A. Aronov (World Scientific, Singapore, 1992), p. 167.

[6] K. Nakajima, H. Mizusawa, H. Sugahara, and Y. Sawada, IEEE Trans. Appl. Supercon. **AS-1**, 29 (1991).

[7] R. Monaco, S. Pagano, and G. Costabile, Phys. Lett. A **131**, 122 (1988).

[8] A. Davidson, N. Grønbech-Jensen, and N. F. Pedersen, IEEE Trans. Magn. **MAG-27**, 3347 (1991).

[9] M. Cirillo, I. Modena, F. Santucci, P. Carelli, and R. Leoni (unpublished).

[10] R. Kleiner, F. Steinmeyer, G. Kunkel, and P. Müller, Phys. Rev. Lett. **68**, 2394 (1992).

[11] In contrast, the Y-Ba-Cu-O compounds show much weaker anisotropy, thus the system may be described by the three-dimensional London or Ginzburg–Landau approach with an anisotropic effective mass tensor; see L. J. Campbell, M. M. Doria, and V. G. Kogan, Phys. Rev. B **38**, 2439 (1988) and L. N. Bulaevskii, V. L. Ginzburg, and A. A. Sobyanin, Sov. Phys. JETP **68**, 1499 (1988).

[12] L. Bulaevskii and J. R. Clem, Phys. Rev. B **44**, 10 234 (1991).

[13] L. N. Bulaevskii, M. Ledvij, and V. G. Kogan, Phys. Rev. B **46** 366 (1992), and references therein. This paper was published after the sub-

2417   J. Appl. Phys., Vol. 73, No. 5, 1 March 1993

Sakai, Bodin, and Pedersen   2417

mission of our present paper. We knew of it thanks to a comment by the referee.

[14] W. E. Lawrence and S. Doniach, in *Proceedings of the 12th International Conference on Low Temperature Physics, Kyoto, Japan*, edited by E. Kanda (Keigaku, Tokyo, 1971), p. 361.

[15] N. F. Pedersen, in *Solitons*, edited by A. A. Maradudin and V. H. Agranowich (North-Holland, Amsterdam, 1986), p. 469.

[16] P. R. Auvil and J. B. Ketterson, J. Appl. Phys. **61**, 1957 (1987).

[17] S. Sakai, H. Akoh, and H. Hayakawa, Jpn. J. Appl. Phys. **24**, L771 (1985).

[18] P. S. Lomdahl, O. H. Sørensen, and P. L. Christiansen, Phys. Rev. B **25**, 5737 (1982).

[19] S. Sakai, P. Bodin, and N. F. Pedersen (unpublished).